An unusual pathway of excitation energy deactivation in carotenoids: Singlet-to-triplet conversion on an ultrafast timescale in a photosynthetic antenna

Claudiu C. Gradinaru*†‡, John T. M. Kennis†§, Emmanouil Papagiannakis*, Ivo H. M. van Stokkum*, Richard J. Cogdell¶, Graham R. Fleming§, Robert A. Niederman‖, and Rienk van Grondelle*

*Department of Biophysics and Physics of Complex Systems, Division of Physics and Astronomy, Faculty of Sciences, Vrije Universiteit, 1081 HV Amsterdam, The Netherlands; §Department of Chemistry, University of California, and Physical Biosciences Division, Lawrence Berkeley National Laboratory, Berkeley, CA 94720; ¶Division of Biochemistry and Molecular Biology, University of Glasgow, Glasgow G128QQ, United Kingdom; and ‖Department of Molecular Biology and Biochemistry, Rutgers University, Piscataway, NJ 08854

Edited by Robin M. Hochstrasser, University of Pennsylvania, Philadelphia, PA, and approved December 27, 2000 (received for review October 23, 2000)

Carotenoids are important biomolecules that are ubiquitous in nature and find widespread application in medicine. In photosynthesis, they have a large role in light harvesting (LH) and photoprotection. They exert their LH function by donating their excited singlet state to nearby (bacterio)chlorophyll molecules. In photosynthetic bacteria, the efficiency of this energy transfer process can be as low as 30%. Here, we present evidence that an unusual pathway of excited state relaxation in carotenoids underlies this poor LH function, by which carotenoid triplet states are generated directly from carotenoid singlet states. This pathway, operative on a femtosecond and picosecond timescale, involves an intermediate state, which we identify as a new, hitherto uncharacterized carotenoid singlet excited state. In LH complex-bound carotenoids, this state is the precursor on the reaction pathway to the triplet state, whereas in extracted carotenoids in solution, this state returns to the singlet ground state without forming any triplets. We discuss the possible identity of this excited state and argue that fission of the singlet state into a pair of triplet states on individual carotenoid molecules constitutes the mechanism by which the triplets are generated. This is, to our knowledge, the first ever direct observation of a singlet-to-triplet conversion process on an ultrafast timescale in a photosynthetic antenna.

Carotenoids (Cars) serve a variety of functions in biological systems. In photosynthesis, they act as light-harvesting (LH) pigments by absorbing sunlight in the blue and green parts of the solar spectrum and transferring the excited state energy to nearby (bacterio)chlorophylls (BChl) (1, 2). The BChl molecules subsequently transfer this energy to a photochemical energy-converting protein known as the reaction center (RC), where the excited state energy is fixed by means of a series of electron transfer reactions (3). During these energy- and electron-transfer processes, which may take up to hundreds of picoseconds, the singlet excited and charge-separated states of BChl are subject to intersystem crossing to the triplet state, which occurs on a timescale of several nanoseconds. Although produced with a small probability, these BChl triplet states are potentially harmful to the organism because they can promote molecular oxygen to its singlet excited state, which is a highly reactive and damaging species. Cars can efficiently accept and safely dissipate BChl triplet and singlet oxygen states, and this photoprotective quality is utilized by essentially all photosynthetic organisms (1, 2).

The first singlet excited state of Cars, S_1, carries gerade symmetry (with respect to inversion) as does the ground state, S_0, and is therefore dipole-forbidden. The second excited singlet state, S_2, carries ungerade symmetry and is dipole-allowed (1). The specific strong Car absorption in the blue and green regions of the visible part of the electromagnetic spectrum is caused by the transition to this second excited state, S_2. On absorption of a photon, fast internal conversion (IC) from the S_2 state to the S_1 state usually takes place in less than 200 fs, then IC from the S_1 state to the ground state occurs on a picosecond timescale (1, 2). Efficient LH by Cars requires these decay channels to be counteracted by faster energy transfer to nearby BChl molecules, and indeed, the efficiency of this process can be as high as 95% (2).

Not all photosynthetic organisms use efficient LH through their Cars. In fact, the first ever demonstration of excitation energy transfer (EET) in a photosynthetic antenna by Duysens in 1952 involved a Car, spirilloxanthin (Spx), in the purple photosynthetic bacterium *Rhodospirillum rubrum*, which transfers only about 35% of the absorbed energy to BChl (4). In another landmark experiment, Rademaker *et al.* measured an unusually high Car triplet yield of ≈30% on direct photoexcitation of Spx in *R. rubrum*, which was strongly reduced upon BChl excitation, thus pointing at a singlet-to-triplet conversion process other than the usual, aforementioned pathway of BChl intersystem crossing followed by triplet energy transfer to Car (5). Later studies indicated that this conversion process was complete in less than 100 ps (6, 7), but assigning a physical origin to this process remained elusive.

In this work, we have investigated this unusual singlet-to-triplet conversion process. We present the results of a femtosecond study of the excited state dynamics of Spx both in solution and in the LH1 complex of *R. rubrum*. Our goal was to identify the intermediate states in the triplet generation pathway in *R. rubrum* and to elucidate its underlying mechanism. It is shown that a new excited state of Spx is generated, both in solution and in the LH1 complex. In the latter case, triplet states are formed from this new state on a picosecond timescale. An assignment of the new electronic state and of the coupling to the triplet state is put forward; the involvement of BChl excited states and the role of the LH1 protein in this process are also discussed. Our results raise fundamental questions regarding the excited-state manifold of Cars and about the factors determining either their efficient LH function or the excited state energy deactivation of these molecules when embedded in photosynthetic proteins.

Materials and Methods

Sample Preparation. The LH apparatus of *R. rubrum* is relatively simple and comprises only one antenna complex, referred to as

This paper was submitted directly (Track II) to the PNAS office.

Abbreviations: Car, carotenoid; BChl, bacteriochlorophyll; LH, light harvesting; Spx, spirilloxanthin; TA, transient absorption; SADS, species-associated difference spectrum; ESA, excited-state absorption; EET, excitation energy transfer; RC, reaction center; RT, room temperature; IC, internal conversion.

†C.C.G. and J.T.M.K. contributed equally to this work.

‡To whom reprint requests should be addressed. E-mail: klaus@nat.vu.nl.

The publication costs of this article were defrayed in part by page charge payment. This article must therefore be hereby marked "*advertisement*" in accordance with 18 U.S.C. §1734 solely to indicate this fact.

www.pnas.org/cgi/doi/10.1073/pnas.051501298

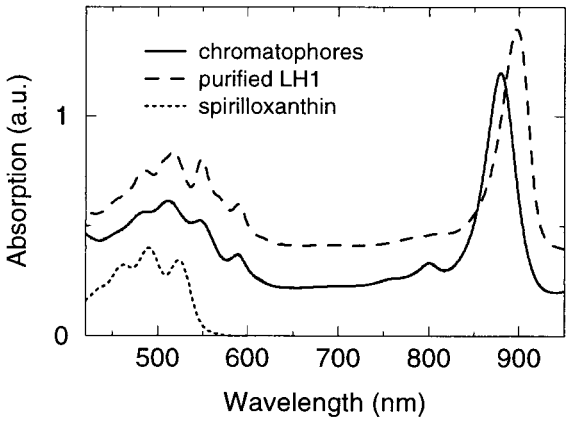

Fig. 1. The absorption spectra of the *R. rubrum* membrane fragments at RT (solid line), purified LH1 complexes at 77 K (dashed line), and extracted Spx dissolved in *n*-hexane at RT (dotted line).

LH1, which surrounds the RC and consists of a ring-like array of 16 $\alpha\beta$-polypeptide subunits, each binding a pair of BChls and one Spx (8). Membrane fragments from *R. rubrum* S1 were prepared as described in (9). Isolated LH1 complexes devoid of RCs were obtained as described in (10). A HPLC assay indicated that exclusively BChl *a* and Spx were present in this preparation. The absorption spectra of both *R. rubrum* preparations are shown in Fig. 1. BChl Q_x and Q_y bands are located near 590 and 880 nm, respectively, whereas Car absorption peaks at 550, 520, and 485 nm. Fluorescence excitation spectra indicated an efficiency of 35% for Car $\rightarrow$ BChl EET in purified LH1 samples as well as membrane fragments (Q. Hu and R.A.N., unpublished results). Spx was extracted from stationary cultures of *R. rubrum* cells as described in ref. 11, which implies the absence of Spx precursors. The absorption spectrum in *n*-hexane is also shown in Fig. 1. For pump–probe experiments, Spx in *n*-hexane was inserted in a sealed 1-mm static cell. The membrane fragments were dissolved in a 50 mM Tris buffer (pH 7.5) to an optical density of around 0.5 per mm in the BChl Q_y band, loaded into a flow system, and circulated by means of a peristaltic pump. The LH1 sample was measured at 77 K, for which the buffer also contained glycerol (70%, v/v) as cryoagent.

Laser Spectroscopy. Femtosecond transient absorption (TA) spectroscopy was carried out with an amplified Ti:sapphire laser system (B.M.I., Cedex, France) operating at 1 kHz, equipped with a home-built noncollinear optical parametric amplifier (NOPA) described in detail earlier (12). We used 25–50 nJ of the NOPA output at 540 nm (17–20 nm width and 40–50 fs duration) to pump the Car S_2 transition. A femtosecond white-light continuum served as probe and reference beams, which were spectrally dispersed and projected onto a home-built double-diode array detection system. For each sample, two sets of data were combined to a final probe window between 470 and 720 nm, to monitor absorption changes in the S_1 and S_2 regions of Spx. The BChl Q_y region (820–950 nm) was probed as well. In all cases, around 200 delay points were sampled, with an average of $\approx$5,000 shots per delay, covering a total delay of 200 ps. Pump and probe beams were linearly polarized, at the magic angle (54.7°) with respect to each other.

Data Analysis. The time-resolved spectra were analyzed with a global fitting program, as described in ref. 13. Species-associated difference spectra (SADS) were determined assuming a sequential irreversible model A $\rightarrow$ B $\rightarrow$ C $\rightarrow$ D. The arrows symbolize increasingly slower monoexponential decays, with time constants that can be regarded as the species lifetimes. This procedure enables us to visualize clearly the evolution of the excited states in the system, although the calculated SADS need not be associated with "pure" molecular states. The instrument response function, fitted with a Gaussian profile, featured a full-width-at-half-maximum of $\approx$100 fs, whereas the group velocity dispersion in the white-light continuum was fitted to a third-order polynomial function of the wavelength.

Results and Discussion

Spirilloxanthin Dynamics in Solution: A New Excited State. We first present the results from Spx extracted from photosynthetic membranes of *R. rubrum*, dissolved in hexane. Spx is the longest naturally occurring Car, with a conjugated polyene chain consisting of 13 double bonds. Its absorption spectrum in hexane (Fig. 1) exhibits maxima at 462, 490, and 525 nm. We collected time-resolved spectra by exciting the sample with 50-fs flashes at 475 nm and probing with a white-light continuum, with a time range from -2 to 100 ps. Rather than presenting the time-resolved spectra themselves, we show the results of a global analysis of these data. Three components were required for an adequate description of the time-resolved data, with lifetimes of 100 fs, 1.4 ps, and 6 ps (Fig. 2*A*). Each species is characterized by a difference spectrum (so-called SADS) relative to the ground-state absorption, a rise time, and a decay time. The dashed spectrum represents the initial absorption change, determined from the raw data after correction for the group-velocity chirp in the probe light and deconvolution with the instrument response function. It displays pronounced ground-

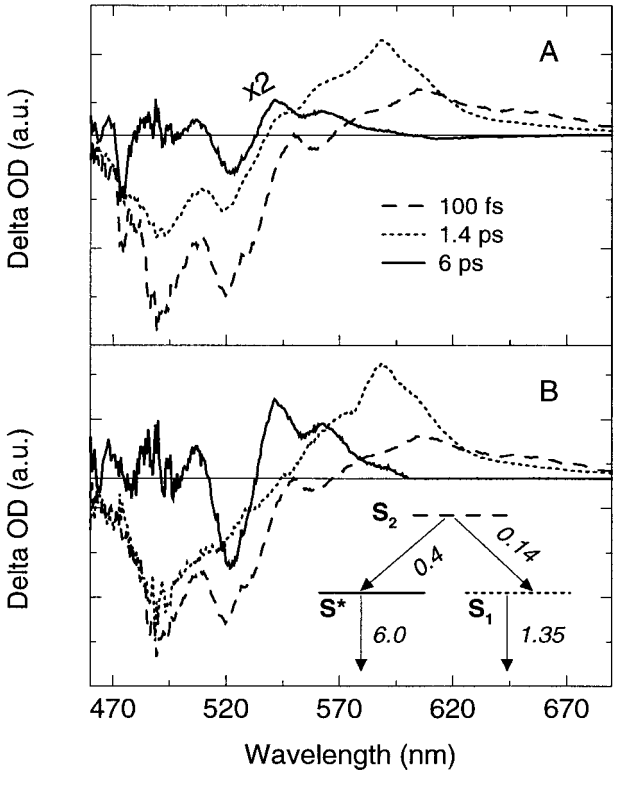

Fig. 2. (*A*) SADS and associated lifetimes for Spx in *n*-hexane upon 475-nm excitation at RT. Note that the third SADS has been expanded by a factor of 2. (*B*). Target analysis by using the kinetic model shown (*Inset*). The arrows indicate exponential decays, with the numbers being the corresponding lifetimes, in picoseconds. The spectra represent the difference absorption of each state (S_2, S_1, and S*), normalized to a concentration of unity. The spectrum of S* was set to zero above 605 nm (see text for details).

state bleaching near 490 and 520 nm, which coincides with the Spx absorption bands. Its lifetime is very short, ≈100 fs, characteristic for the S_2 state of Cars (1, 2). It is therefore straightforward to assign this SADS to the initially excited S_2 state of Spx, and the 100-fs lifetime to the depopulation of this state.

The initially excited state (S_2) decays to a second species, which lives for 1.4 ps. The SADS of this intermediate (dotted line) has a bipolar shape, consisting of two ground-state bleaching peaks at 490 and 520 nm and a strong excited-state absorption (ESA) at 590 nm. The ESA at 590 nm is related to the presence of the optically forbidden S_1 state. It is well known that S_1 is formed from the S_2 state via IC on a femtosecond timescale, and that the spectroscopic signature of this dark state in Cars is a large absorption cross section to higher excited states, which is red-shifted with respect to the ground-state absorption (1, 14). We conclude that the lifetime of the Spx S_1 state is 1.4 ps, which is in agreement with the value inferred by extrapolating kinetic data obtained for shorter Cars (2).

The third SADS (solid line), having a smaller amplitude and a lifetime of 6 ps, shows a bleaching around 520 nm, a main ESA peak at 542 nm, and a minor one at 564 nm. Note that the salient features of this SADS, especially the 542-nm ESA band, seem to be already present in the second SADS. The absence of long-lived components indicates that no detectable amount of Spx triplets was formed in solution, in contrast to the situation in LH1 of *R. rubrum* (5), but in agreement with earlier flash photolysis experiments (15). We emphasize that the 6-ps signal cannot be caused by a contamination by Spx precursors with a shorter conjugated chain length, because the sample originated from stationary cultures of *R. rubrum* (11).

These data demonstrate that Spx in solution does not display the usual biexponential Car dynamics, i.e., relaxation in 100–200 fs from the S_2 to S_1 state followed by relaxation of the latter to the ground state on a picosecond timescale (1, 2). A third species is formed, which has a longer lifetime than the S_1 state and is spectrally distinct from it. This species is associated with a state additional to S_1 and S_2, which we call S*. Importantly, it has characteristic features—ESA bands at 542 and 564 nm—that are already present during the lifetime of the S_1 state (i.e., in the second SADS). This observation suggests that S* is formed directly from S_2, in parallel with the formation of S_1.

To uncover the difference spectra of the pure states S_2, S_1, and S*, which seem to coexist in the sequential model, we applied a so-called target analysis (16) to our data. We assumed the kinetic model depicted in Fig. 2*B*, by which S_2 has two parallel decay pathways, into S_1 and S*. Note that in Fig. 2*A*, the longest-lived species (solid line) has no ESA at wavelengths longer than 605 nm. The branching between S_1 and S* can be determined by requiring the S* spectrum to be zero in this wavelength range during all times. This requirement results in 70% of the S_2 states to decay to S_1 and 30% to S*. The spectra of the three states (S_2, S_1, and S*) that follow from the target analysis are shown in Fig. 2*B*. The spectrum of the S_2 state is identical to the initial SADS in the sequential model (Fig. 2*A*), as is expected. The spectrum of the S_1 state has an ESA maximum at 590 nm, like the second SADS in the sequential model (Fig. 2*A*, dotted line), but it lacks the ESA feature at 542 nm. Its overall shape agrees well with the S_1 spectra reported earlier (14), and around 490 nm it is almost identical to the S_2 spectrum, as expected for ground-state bleaching. The S* spectrum is clearly distinct from that of S_1 and exhibits positive peaks at 542 and 564 nm and a bleaching at 520 nm.

What could be the nature of the S* state? A "hot" ground state can, in principle, cause the absorption features at 542 and 564 nm (14), but then one would also expect a bleaching at 490 nm. Cooling of a "hot" S_1 excited state would produce a blue shift and a spectral narrowing, which we observe on going from the second to the third SADS in Fig. 2*A*, but this process should be conservative with respect to ESA by S_1, which is clearly not the case. Moreover, the lifetime associated with the second SADS, 1.4 ps, closely agrees with what one should expect from a Car of this length (2). A possible partition of the Car S_1 states into "fast" and "slow" decaying is discarded by the shape of the "slow" spectrum, unusual when compared to literature data (1, 12, 14). It thus appears extremely likely that S* is a hitherto uncharacterized electronic state of Spx, lying somewhere below S_2, and being one-photon forbidden. This dark state could be the Car $1B_u^-$ state found recently in sphaeroidene crystals (17), which satisfies both conditions above. In analogy to the dynamical twisting of retinal in rhodopsins (18), and considering the apparent absence of an equilibrium between S_1 and S*, these states could also reflect different molecular configurations of Spx, separated by an energy barrier.

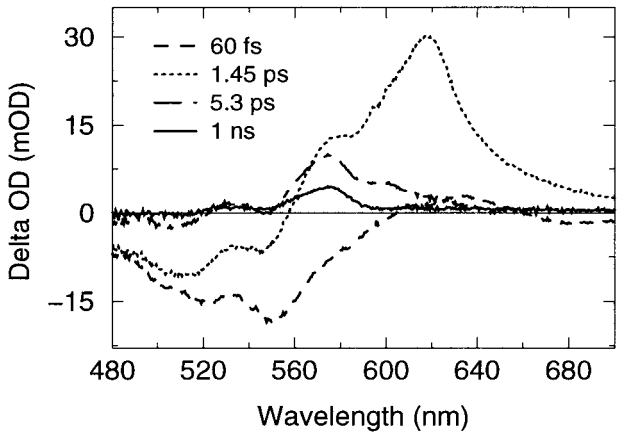

Fig. 3. SADS and lifetimes characterizing the spectral evolution of the TA induced by 540-nm excitation in membrane fragments from *R. rubrum,* at RT. The species generated by the laser pulse (dashed) is replaced with a time constant of 60 fs by the next one (dotted), which in turn decays in 1.45 ps into the dot-dashed spectrum. This species evolves in ≈5.3 ps into a long-lived species (solid), whose lifetime was set to 1 ns in the global analysis.

Car Excited-State Dynamics in Membrane Fragments from *R. rubrum*. As mentioned in the Introduction, it was shown by Rademaker *et al.* that on direct Spx excitation in *R. rubrum*, Spx triplets are generated with a high yield (5). We investigated this process by performing femtosecond TA measurements on membrane fragments of *R. rubrum*. The absorption spectrum of these membranes, which contain the entire photosynthetic apparatus including LH1 complexes and RCs, is shown in Fig. 1. Note that the Spx absorption is 25–30 nm red-shifted with respect to Spx in solution. The membranes were excited at 540 nm. The evolution of the TA signals between 480 and 700 nm can be described by four exponentials of 60 fs, 1.45 ps, 5.3 ps, and a long-lived end level, with the corresponding SADS displayed in Fig. 3.

The initial spectrum (dashed line) shows distinct bleaching features near 520 and 550 nm, which match the Spx S_2 bands in LH1 (Fig. 1). Its lifetime is 60 fs, which is shorter than Spx in solution (100 fs). This value is characteristic for the Car S_2 state in the presence of EET to BChls (12, 19), thus implying that Car → BChl excitation transfer in the LH1 complex of *R. rubrum* proceeds from the S_2 state.

The initially excited state (S_2) decays in ≈60 fs to the next state, which lives for 1.45 ps. The SADS of this intermediate (dotted line) has a bipolar shape and is very similar to that observed for Spx in solution (Fig. 2*A*, dotted line). It consists of two bleaching peaks at 512 and 545 nm, a strong ESA maximum at 620 nm, and a pronounced shoulder near 575 nm. The ESA

maximum at 620 nm is caused by the S_1 state of Spx, formed via IC from the S_2 state. Note that the bleaching peaks at 512 and 545 nm are diminished when compared to the previous SADS, which can be explained by Car → BChl excitation transfer from the S_2 state. The S_1 lifetime in the LH1 complex, 1.45 ps, is essentially the same as in solution (see Fig. 2), suggesting that besides IC to the ground state, no additional loss channels, such as EET to BChl, are active for the S_1 state of LH1-bound Spx. Very conspicuous is the presence in the second SADS of an ESA feature near 575 nm, which corresponds to the position of the S* state in Spx in solution (Fig. 2*B*), when taking into account the red shift of the absorption spectrum in the protein. It thus appears that S* is also formed in the LH1–RC complex, in direct correlation with the deactivation of the S_2 state. As in solution, the second SADS seems to have contributions of both the S_1 and the S* states. Intriguingly, 575 nm is also the wavelength where the Spx triplet state in *R. rubrum* shows maximal absorption (ref. 5; see also below).

The third SADS (dash-dotted line) has a lifetime of 5.3 ps, and its main characteristics are ESA peaks at 575 and 600 nm. Its amplitude is negligible for wavelengths longer than 640 nm, and a small positive feature is present near 535 nm. Both the shape of the spectrum and the lifetime of this state are similar to those observed for Spx S* state formed in solution (Fig. 2*A*, solid line). This observation thus provides definite evidence that S* is formed in the LH1 complex of *R. rubrum* as well.

The fourth SADS (solid line) is essentially nondecaying on the timescale of our experiment, but for convenience its lifetime was set to 1 ns in the analysis. It has one single ESA maximum at 575 nm. This SADS is virtually identical to the Spx triplet spectrum measured by Rademaker *et al.* on a microsecond timescale (5), and we accordingly assign it to the Spx triplet state T_1. It thus appears that after 5.3 ps, a fraction of the excitations has reached the Spx triplet state. This, to our knowledge, is the first ever direct observation of the appearance of Car triplet states on such an ultrafast timescale. Strikingly, the third SADS, which we assign to the S* state, and the fourth SADS, assigned to the T_1 state in *R. rubrum*, bear marked spectral similarities. This resemblance is a strong indication that S* is an intermediate state on the pathway to the Spx T_1 state. With respect to the third SADS, the 575-nm peak has decreased by ≈50%, and the 600-nm ESA peak has disappeared.

Purified LH1 Preparations. Pump–probe measurements performed on purified detergent-solubilized LH1 complexes devoid of RCs show an almost identical spectral evolution compared to membrane fragments (Fig. 4*A*). The low temperature conditions resulted in a better resolution of various spectral features, but the characteristic lifetimes remained the same: ≈70 fs, 1.6 ps, 5 ps, and 1 ns. This similarity demonstrates beyond doubt that the observed triplet state resides on an antenna Car rather than in the RC, and that all the intermediate steps leading to the triplet state occur in the antenna. These data reveal once more, with enhanced clarity, that the S* absorption band near 575 nm is already present in the second SADS (dotted line), immediately after the 70-fs decay of S_2.

No Role of BChl in the Triplet Generation. It has been argued before that BChl molecules in the LH1 ring could be involved in the triplet conversion process, through either a radical pair or a triplet pair mechanism (5). In the first case, a charge separation may take place between the excited Spx and a BChl. Provided that the lifetime of the charge-separated state would be long enough for intersystem crossing to occur, i.e., in the order of nanoseconds, the resulting charges could recombine to form the Car triplet state. However, we observed that the Spx triplet is formed within picoseconds, and we may thus safely dismiss this mechanism. The second possibility involves the fission of one

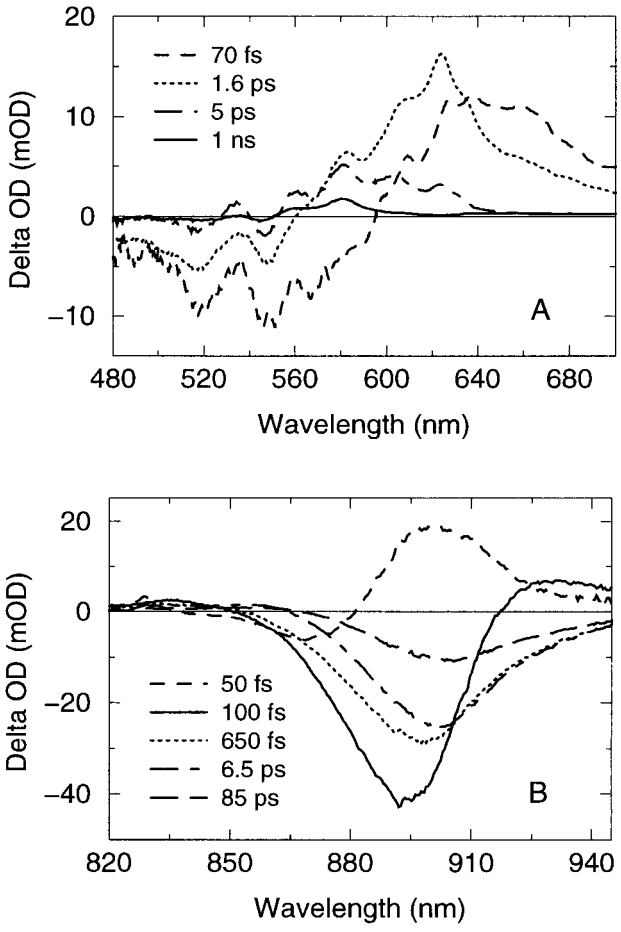

Fig. 4. Global analysis results (SADS and associated lifetimes) of the TA data obtained in the visible (*A*) and near IR (*B*) after 540 nm excitation in purified LH1, at 77 K.

singlet excitation into a pair of triplets, yielding one Car and one BChl triplet, a mechanism referred to as heterofission. For such a pathway, specific changes of the BChl absorption should appear on a (sub)picosecond timescale, correlated with the spectral evolution in the Car region.

To check for the possible involvement of BChl in the triplet formation process, we performed measurements in the BChl Q_y region in the near infrared (820–950 nm). The evolution of the TA signals on Car excitation at 540 nm excitation in isolated LH1 complexes at 77 K is described by five lifetimes of 50 fs, 100 fs, 650 fs, 6.5 ps, and 85 ps and by the SADS displayed in Fig. 4*B*. The first step (between the first and the second SADS) is a 50-fs rise of BChl bleaching, centered around 894 nm. Given the selective Car excitation, and that the 50-fs time constant is very similar to the Car S_2 decay time, we attribute this event to Car S_2 → BChl Q_x singlet energy transfer. The third SADS (dotted line), which develops in 100 fs, shows the appearance of BChl-stimulated emission above 910 nm, which is indicative of BChl Q_x → Q_y relaxation. During the next 650 fs, an 11-nm red shift of the difference spectrum occurs (fourth SADS). This evolution has been observed previously with direct BChl excitation in *R. rubrum* and was interpreted in terms of excitation equilibration in the inhomogeneously broadened antenna (20). The slower processes (6.5 and 85 ps) are mainly associated with loss of excited states through annihilation and/or quenching channels (20–22).

It thus appears that, apart from the ultrafast Car → BChl EET

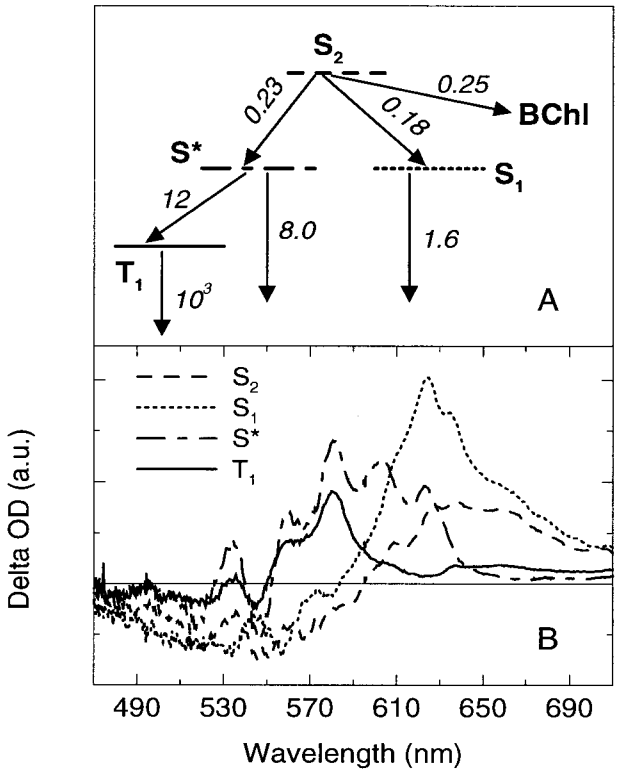

Fig. 5. Target analysis of the TA data obtained for LH1 at 77 K. (*A*) The model used for target analysis. The numbers represent the reciprocals of the microscopic decay rates, in picoseconds. (*B*) The difference spectra associated to the Spx states S_2, S_1, and S* and T_1 from *A*.

in 50 fs, the other events described above reflect only BChl excited-state dynamics, at rates and with spectral characteristics similar to those found on direct excitation of BChl (20). No long-lived species were detected in this spectral window, indicating that no BChl triplet states were formed. In a control experiment, we examined the dynamics in the carotenoidless G9 mutant of *R. rubrum* using excitation at 540 nm. This measurement (not shown) shows long-lived signals at least 10 times smaller than those presented in Fig. 4*A*, unequivocally proving that the latter signals are solely related to Cars.

A Kinetic Model for Singlet–Triplet Conversion on LH1-Bound Spx. On the basis of our results, we propose that the excited-state deactivation of the LH1-bound Spx proceeds via the kinetic scheme depicted in Fig. 5*A*. The main underlying premises of this model are: (*i*) energy transfer to BChl occurs only from S_2 and is ≈30% efficient; (*ii*) radiationless decay from S_2 to the ground state occurs via either S_1 or S*; and (*iii*) the Car triplet is formed only from S*, as implied by the spectral resemblance between the two species. As in Spx in solution, we have applied a target analysis to the time-resolved data of LH1 at low temperature. This approach yielded the SADS of the four pure states, S_2, S_1, S*, and T_1, which are shown in Fig. 5*B*. Most remarkable is the separation of the ESA contributions caused by S_1 around 620 nm and S* at 575 nm, which coexisted in the sequential picture (Fig. 4*A*, second SADS). Now, the S_1 spectrum (dotted line) has one positive peak at 625 nm, a featureless blue wing, and a long tail to the red. In contrast, the S* spectrum (dot-dashed line) shows distinct ESA peaks at 560, 580, and 600 nm (and 625 nm) with little amplitude further to the red. The branching of the S_2 deactivation could not be solved, but a ratio of relative concentrations of $Q_x/S_1/S^*$ close to 0.3/0.4/0.3 gave a good resemblance of the S_1 and S_2 spectra below 560 nm, where they are expected to show similar ground state bleachings (dashed and dotted lines).

The Car S* state in LH1 displays the same basic features as in hexane, i.e., a lifetime of 5 ps, a sharp bleaching of the red-most ground state absorption band, and a sequence of ESA peaks on the long-wavelength side, whereas the S_1 spectrum estimated by the target analysis has the shape of a typical Car S_1 spectrum (1, 14). These facts support our model description of the deactivation of the S_2 state, consisting of two alternative pathways. The Spx triplet appears in the LH1 antenna on a picosecond timescale, one of the assumptions of the model being that this long-lived state is formed via S*. This idea is justified by the close spectral resemblance between the two species: apart from the ESA peaks at 605 and 625 nm of S*, every other feature is conserved: bleach signals centered at 480, 515, and 545 nm, and predominant ESA near 535, 560, and 580 nm (Fig. 5*B*). In addition, the S_1 lifetimes are almost identical in solution and in the LH1 complex, indicating that the depopulation of this state should be exclusively ascribed to IC to the ground state.

Magnetic field measurements on *R. rubrum* samples have shown that field intensities in the order of 0.5 T induce a decrease by ≈40% of the Car triplet yield (5) and only a small increase of the yield of BChl fluorescence (<0.2%) (23). These results implicate a separation between the triplet generation and singlet energy transfer pathways, thus confirming the first two assumptions of the target analysis. Moreover, the large magnetic field effect on the triplet yield discards intersystem crossing as a possible mechanism for singlet–triplet conversion, because the efficiency is of this process is basically independent of magnetic field. This pathway requires spin-orbit-mediated spin dephasing, which is typically a "slow" process (nanosecond range), whereas our data show unambiguously that in *R. rubrum*, LH1 Spx triplet states are formed in at most 5 ps on selective excitation of this pigment.

Mechanism of Triplet Formation. A mechanism that has been proposed to explain the magnetic field data is singlet exciton fission (5), known to occur in organic crystals (24) and in conjugated polymers such as poly-diacetylene (25). This phenomenon involves the dissociation of a singlet state to a pair of triplet states $T^{(1)}$ and $T^{(2)}$, whose spins, with net magnetic moments given by the quantum numbers −1, 0, and +1 (indicated as subscripts), are coupled to an overall singlet state ^1S (26):

$$^1S = \frac{1}{\sqrt{3}}(T_1^{(1)}T_{-1}^{(2)} - T_0^{(1)}T_0^{(2)} + T_{-1}^{(1)}T_1^{(2)}) .$$

Triplet formation on adjacent Spx molecules is unlikely to occur, given their large separation in the LH1 structure (≈20 Å, ref. 8). Instead, we explain our results by asserting that two triplets are generated on an individual Car molecule but are localized on different parts of it. This mechanism is referred to as intramolecular homofission. Theoretical studies of polyenes have shown that their covalent excitations (the "–" states) can be decomposed into irreducible products of triplet excitations (26). For instance, the covalent S_1 state ($2^1A_g^-$) has been characterized as a doubly excited, spin-correlated triplet state $1^3B_u \otimes 1^3B_u$. This view is supported by the fact that for many Cars, the energy of the lowest triplet, T_1, is about half that of the S_1 state (1, 2).

In our case, however, S_1 exhibits an identical behavior irrespective of the triplet generation, and therefore it seems logical that this state is not the parent singlet from which the fission occurs. In our interpretation of the experimental data, S* is the precursor state for the triplet formation. Theoretical calculations applied to long polyenes predicted that other covalent excita-

tions (e.g., $1^1B_u^-$, $3^1A_g^-$, etc.) will be situated below the ionic $1^1B_u^+$ (S_2) state (26). Thus, S* might be one of these "–" states, having the character of multiple triplet excitations. Tavan and Schulten emphasized that the probability of a covalent singlet dissociating into its triplet constituents is strongly enhanced by distortions of the polyenal chain (26). This effect would explain why in hexane, where the Spx molecule is not distorted, the S* state relaxes to the ground state and no triplets are observed. When inserted into the LH1 antenna the Car experiences a quite asymmetric environment, which may induce twisting of the polyene chain by specific Car–protein interactions inducing localization of the triplets. Judging from the amplitude of the last two SADS from Figs. 3*A* and 4*A*, there is ≈50% chance that the triplets dissociate before the S* relaxes to the ground state, in about 5 ps. The large size of the conjugated backbone of Spx (13 double bonds) may be an important property in accommodating the two localized triplets.

There is an interesting analogy with Cars that do have an efficient LH function. The same symmetry-breaking elements that in the case of *R. rubrum* result in triplet localization have been proposed in these Cars to give the dark S_1 state enough Coulombic character to electronically couple with nearby BChls and thus enable EET between these pigments (27). It is unclear, however, whether the S_1 state in Spx in *R. rubrum* would have such enhanced Coulombic character as well: its LH function is not active because of the short S_1 lifetime of 1.4 ps and, possibly, Spx's poor spectral overlap with LH complex-bound BChl.

Comparing the magnitude of our TA signals with the extinction coefficients from the literature (28, 29), we estimate that the triplet yields are ≈25% for LH1 at 77 K, and ≈35% for the chromatophores at room temperature (RT). The target analysis provided an upper limit of 30%, somewhat in discrepancy with that reported by Rademaker *et al.* (15%, using the triplet extinction coefficient from ref. 28). It is possible that in the latter case, loss processes, such as intra- or intermolecular triplet–triplet annihilation, have occurred faster than their time resolution of 1 μs.

In terms of photosynthetic activity, the singlet fission pathway is nonproductive, and it may well be that it has no biological significance. Most probably, Spx has been selected by the organism for photoprotection rather than for LH.

Concluding Remarks

This work demonstrates that an ultrafast, unconventional singlet-to-triplet conversion on the Car bound to the photosynthetic antenna protein (LH1) of the purple bacterium *R. rubrum* is at the basis of its poor LH function. Following the unusual pattern of the excited state dynamics of spirilloxanthin in solution and inspired by theoretical calculations of polyene excitations (26), we propose that the triplets are generated through fission from a new Car singlet state, S*. Since the triplet and S* spectra share many common features, it is argued that S* belongs to a class of Car excitations known as covalent, which are commonly described as a combination of triplet excitations. In the protein environment, the long Spx molecule is probably distorted from its symmetric configuration, a situation that favors the dissociation of S* into the constituent triplets, whereas in solution S* decays directly to the ground state in ≈5 ps. It thus appears that triplets are present in LH1 approximately 100 fs after selective Car photoexcitation, at first coupled in pairs to a singlet state, S*, and then separated, on a picosecond timescale, after the fission event. Finally, this study has shown that occurrence of triplet states on the ultrafast timescale is determined both by the electronic structure of Spx and the structural perturbation dictated by the protein environment. To disentangle these influences and to investigate the universality of this process in photosynthetic systems, experiments on a variety of LH complexes with designed Car content will prove crucial.

We are grateful to Prof. Klaus Schulten for insightful discussions. This project was supported by the Netherlands Organization for Scientific Research through the Council of Earth and Life Sciences (R.v.G.) and by the Charles and Johanna Busch Memorial Fund (R.A.N.). C.C.G. and J.T.M.K. acknowledge the Human Frontier Science Program Organization for financial support.

1. Koyama, Y. & Hashimoto, H. (1993) in *Carotenoids in Photosynthesis*, eds. Young, A. & Britton, G. (Chapmann & Hall, London), pp. 327–409.
2. Koyama, Y., Kuki, M., Andersson, P. O. & Gillbro, T. (1995) *Photochem. Photobiol.* **63,** 243–256.
3. van Grondelle, R., Dekker, J. P., Gillbro, T. & Sundstrom, V. (1994) *Biochim. Biophys. Acta* **1187,** 1–65.
4. Duysens, L. N. M. (1952) Ph.D. thesis (University of Utrecht, Utrecht, The Netherlands).
5. Rademaker, H., Hoff, A. J., van Grondelle, R. & Duysens, L. N. M. (1980) *Biochim. Biophys. Acta.* **592,** 240–257.
6. Nuijs, A. M., van Grondelle, R., Joppe, H. L. P., van Bochove, A. C. & Duysens, L. N. M. (1985) *Biochim. Biophys. Acta* **810,** 94–105.
7. Hayashi, H., Kolaczowski, S. V., Noguchi, T., Blanchard, D. & Atkinson, G. H. (1990) *J. Am. Chem. Soc.* **112,** 4664–4670.
8. Karrash, S., Bullough, P. A. & Ghosh, R. (1995) *EMBO J.* **14,** 631–638.
9. Inamine, G. S. & Niederman, R. A. (1982) *J. Bacteriol.* **150,** 1145–1153.
10. Picorel, R., Bélanger, G. & Gingras, G. (1983) *Biochemistry* **22,** 2491–2497.
11. Lozano, R. M., Manzano, I., Gomez, R. & Ramirez, J. M. (1989) *Biochim. Biophys. Acta* **976,** 196–202.
12. Gradinaru, C. C., van Stokkum, I. H. M., Pascal, A. A., van Grondelle, R. & van Amerongen, H. (2000) *J. Phys. Chem.* **104,** 9330–9342.
13. Van Stokkum, I. H. M., Scherer, T., Brouwer, A. M. & Verhoeven J. W. (1994) *J. Phys. Chem.* **98,** 852–866.
14. Andersson, P. O. & Gillbro, T. (1995) *J. Phys. Chem.* **103,** 2509–2519.
15. Bensasson, R., Land, E. J. & Maudinas, B. (1976) *Photochem. Photobiol.* **23,** 189–193.
16. Holzwarth, A. R. (1996) in *Biophysical Techniques in Photosynthesis,* eds. Amesz, J. & Hoff, A. J. (Kluwer, Dordrecht, The Netherlands), pp. 75–92.
17. Sashima, T., Nagae, H., Kuki, M. & Koyama, Y. (1999) *Chem. Phys. Lett.* **299,** 187–194.
18. Gai, F., Hasson, K. C., McDonald, J. C. & Anfinrud, P. A. (1998) *Science,* **279,** 1886–1891.
19. Krueger, B. P., Scholes, G. D., Jimenez, R. & Fleming, G. R. (1998) *J. Phys. Chem.* **102,** 2284–2292.
20. Visser, H. M., Somsen, O. J. G., van Mourik, F., Lin, S., van Stokkum, I. H. M. & van Grondelle, R. (1995) *Biophys. J.* **69,** 1083–1099.
21. Valkunas, L., Åkesson, E., Pullerits, T. & Sundström, V. (1996) *Biophys. J.* **70,** 2373–2379.
22. Monger, T. G., Cogdell, R. J. & Parson, W. W. (1976) *Biochim. Biophys. Acta* **449,** 136–153.
23. Kingma, H. M., van Grondelle, R. & Duysens, L. N. M. (1985) *Biochim. Biophys. Acta* **808,** 363–382.
24. Geacintov, N. E., Pope, M. & Vogel, F. (1969) *Phys. Rev. Lett.* **22,** 593–596.
25. Kraabel, B., Hulin, D., Aslangul, C., Lapersonne-Meyer, C. & Schott, M. (1998) *Chem. Phys.* **227,** 83–98.
26. Tavan, P. & Schulten, K. (1987) *Phys. Rev. B* **36,** 4337–4357.
27. Damjanovic, A., Ritz, T. & Schulten, K. (1999) *Phys. Rev. E* **59,** 3293–3311.
28. Cogdell, R. J., Land, R. J. & Truscott, T. G. (1983) *Photochem. Photobiol.* **38,** 723–725.
29. Arellano, J. B., Bangar Raju, B., Razi-Naqvi, K. N. & Gillbro, T. (1998) *Photochem. Photobiol.* **68,** 84–87.